Brownian Dynamics Simulation of DNA Unrolling from the Nucleosome†

T. Wocjan,‡ K. Klenin,§ and J. Langowski*,‡

Biophysics of Macromolecules, German Cancer Research Center, D-69120 Heidelberg, Germany, and Institut für Nanotechnologie, Forschungszentrum Karlsruhe GmbH, Postfach 3640, D-76021 Karlsruhe, Germany

Received: July 11, 2008; Revised Manuscript Received: October 14, 2008

Nucleosomes organize chromatin in eukaryotic cells at the lowest scale by wrapping the DNA double helix around a histone octamer. The mechanism by which this structure can be opened, giving access to DNA-processing enzymes, is of fundamental biological importance. Here we describe a new coarse-grained model based on the toroidal geometry of the nucleosome which allows the simulation of nucleosome stretching experiments with a Brownian dynamics algorithm including hydrodynamics. We obtain force-extension curves and calculate energy barriers and kinetic rate constants of the unrolling transition from rupture forces.

Introduction

In eukaryotic cells, DNA is organized into chromatin. Its basic packing unit is the nucleosome core particle, which wraps 146 bp of DNA around a protein complex. The structure of the nucleosome has been resolved at high resolution by X-ray crystallography:[6−8] the nucleosome core is a cylindrical protein aggregate, consisting of two molecules each of the histone proteins H2A, H2B, H3, and H4, and the DNA double-helix making a left-handed superhelix of 1 and $^3/_4$ turns around the histone octamer. The dynamics of the nucleosome between an open state, in which DNA is not sterically occluded inside the nucleosome and can be accessed by proteins responsible for fundamental process as such DNA transcription and replication, and a condensed state, which is characteristic of the compact chromatin fiber, is of fundamental biological importance.

In recent years, single-molecule experiments have been devised which allowed to probe forces at the molecular level. Stretching experiments of optically trapped nucleosomal arrays have shown that a considerable energy barrier hinders the complete unwinding of DNA from the nucleosome.[13,15] Theoretical calculations on an analytical model indicate that the toroidal geometry of the nucleosome itself is of great importance to stabilization of the nucleosome.[14] Here, we developed a model of the nucleosome based on the known geometry and simulate stretching experiments within a Brownian dynamics simulation in order to extract information about the kinetic rates and energy barriers of the unwrapping transition.

The outline of the paper is as follows: In the first section, we describe the model for the DNA polymer and the histone core. In the second section, the details of the Brownian dynamics algoritm and the hydrodynamics are presented. The third section contains the results of the stretching simulation and the analysis of the data.

Theory and Methods

DNA Model. The DNA is based on the model described in (1); here, we give a brief overview and state the basic assumptions underlying the simulation. The simulation parameter values are given in Table 1. The DNA molecule is modeled as an elastic chain with electrostatic interactions. The chain has N straight segments, and the chain conformation is specified by the positions of its vertices, $\vec{r}_i$, $i = 0,..., N$. The segments are represented by the vectors $\vec{s}_i = \vec{r}_{i+1} - \vec{r}_i$, $i = 0,..., N - 1$. To each segment a local coordinate system of three orthogonal vectors of unit length is attached ($\vec{f}_i, \vec{g}_i, \vec{e}_i$), so that the $\vec{e}_i$ direction coincides with the direction of the ith segment: $\vec{e}_i = \vec{s}_i/s_i$, $s_i = |\vec{s}_i|$. The stretching energy is defined for each segment i

$$\frac{E_i^{(s)}}{k_B T} = \frac{1}{2(l_0\delta)^2}(l_0 - s_i)^2 \tag{1}$$

where k_B is the Boltzmann constant, T is the temperature, l_0 is the segment equilibrium length, and δ is the stiffness parameter. For each chain joint a bending energy is defined

$$\frac{E_i^{(b)}}{k_B T} = \alpha_b \beta_i^2 \tag{2}$$

where α_b is the bending rigidity parameter and β_i the angle between $\vec{e}_{i-1}$ and $\vec{e}_i$. The bending rigidity parameter depends upon the Kuhn length B of the polymer according to the following equation

$$\frac{B}{l_0} = \frac{1 + \langle\cos\beta\rangle}{1 - \langle\cos\beta\rangle} \tag{3}$$

where the relationship between B and α_b is given by

$$\langle\cos\beta\rangle = \frac{\int_0^\pi \cos\beta \sin\beta \exp(-\alpha_b\beta^2)\, d\beta}{\int_0^\pi \sin\beta \exp(-\alpha_b\beta^2)\, d\beta} \tag{4}$$

The twist energy between two adjacent segments:

† Part of the "J. Michael Schurr Special Section".

* Corresponding author. Address: Biophysics of Macromolecules, German Cancer Research Center (DKFZ), Im Neuenheimer Feld 280, 69120 Heidelberg, Germany. Phone: +49-6221-42 3990.

‡ German Cancer Research Center.

§ Institut für Nanotechnologie.

10.1021/jp806137e CCC: $40.75
Published on Web 12/05/2008

$$\frac{E_i^{(t)}}{k_B T} = \frac{1}{2k_B T}\frac{C}{l_0}\tau_i^2 \tag{5}$$

where C is the torsional rigidity constant and τ_i is the twist angle between the $(i-1)$th and ith segments. Here the twist angle τ_i is defined as the sum $\tau_1 + \tau_2$, where τ_1 is the angle between the local coordinate unit vector $\vec{f}_{i-1}$ and the vector $\vec{p}_i = \vec{s}_{i-1} \times \vec{s}_i$, which is normal to the segment vectors, and the second angle τ_2 between $\vec{p}_i$ and $\vec{f}_i$. The electrostatic interaction between the DNA segments in this model is treated within the Debye−Hückel approximation. The electrostatic contribution to the energy for two nonadjacent DNA segments (i, j) in a monovalent salt solution is

$$\frac{E_{ij}^{(e)}}{k_B T} = \frac{\upsilon^{*2}}{k_B T D}\int d\lambda_i \int d\lambda_i \frac{\exp(-\kappa r_{ij})}{r_{ij}} \tag{6}$$

Here κ^{-1} denotes the Debye−Hückel screening length, which is given by $\kappa^2 = 8\pi e^2 I/k_B TD$. The salt solution is specified by the ionic strength I, the proton charge e, and the dielectric constant of water D. In the integration, r_{ij} is the distance between the positions at the two segments, parametrized by the integration parameters λ_i and λ_j. DNA is a highly charged polyelectrolyte with a linear bare charge density $\nu = -2e/\Delta$, where $\Delta = 0.34$ nm is the basepair distance. According to Manning,[21] a condensation of counterions at the polyelectrolyte for highly charged cylinders in salt solutions, such as DNA, occurs above a threshold of the dimensionless linear charge density $\xi^* = l_{Bjerrum}/b = 1$. The Bjerrum length $l_{Bjerrum} = e^2/4\pi D k_B T$ signifies the distance at which two elementary charges interact with thermal energy, and $b = \Delta/2$ is the polymer contour length containing one elementary charge. A certain fraction of counterions stays bound to the charged cylinder even in the limit of infinite dilution, renormalizing the effective dimensionless line charge density to the critical value of unity, so that the renormalized linear charge density $\nu^* = 1/l_{Bjerrum}$ is roughly a quarter of the bare linear charge density. It has to be remarked that the renormalized charge is obtained in the limit of vanishing salt and that in the presence of the positively charged histone core counterions are driven away from the DNA. Therefore the charge renormalization due to counterion condensation sets only a lower bound on the effective linear charge density and it is used to estimate the maximal effect of charge renormalization in the unwrapping process, while the bare linear charge density ν represents an upper bound in the simulations.

Histone Octamer Model. The structure of the nucleosome core particle has been resolved by X-ray crystallography.[6,7] The nucleosome consists of an $(H3-H4)_2$ tetramer, two H2A−H2B dimers forming a fairly rigid protein complex of cylindrical shape. The crystallographic data shows that the DNA in the nucleosome structure makes a flat, left-handed superhelix around the nucleosome core. As illustrated in Figure 6, the histone core in our model is represented as a cylinder with radius $R^{(n)} \sim 4.18$ nm. In order to simulate the adsorption of the DNA to the histone core we assume a phenomenological potential such that the DNA polymer conformation from the experiments is recovered at equilibrium. Thus a superhelical path with $1\ ^3/_4$ turns and a pitch p of 2.39 nm according to the known geometry is defined on the surface of the cylinder. Then the interaction distance $|\vec{R}_i|$ between DNA and protein is determined as the shortest distance between a point on this path and the middle point $\vec{r}_i^{(m)}$ of the ith segment. For physiological conditions as used in the simulations the electrostatic interaction between the DNA chain and the octamer can be considered as short-range. A V-groove potential for the distance dependence is chosen up to a cutoff distance r_0. The cutoff parameter is of the order of the screening length, reflecting the fact that electrostatic interactions between DNA and histone core are of main importance. The interaction energy $E_i^{(n)}$ for each interacting segment can be tuned with the potential depth parameter U_0 or, respectively, the adsorption energy density $\epsilon = U_0/l_0$.

$$\frac{E_i^{(n)}}{k_B T} = \begin{cases} -U_0\dfrac{r_0 - |\vec{R}_i|}{r_0}\left[\dfrac{\Theta_0 - \Theta_i}{\Theta_0}(1-k_0) + k_0\right] & \Theta_i < \Theta_0 \\ -U_0\dfrac{r_0 - |\vec{R}_i|}{r_0}k_0 & \Theta_i \geq \Theta_0 \end{cases} \tag{7}$$

The angle dependency of the potential has a V-groove shape for $\Theta_i < \Theta_0$, while outside the critical angle Θ_0, the potential is constant, reduced by a factor k_0. $\Theta_i = \arccos(\vec{f}_i \cdot \vec{a})$ is defined as the angle between the $\vec{f}_i$ vector, indicating the orientation of the segment, and a vector $\vec{a}$ which takes the twist of the polymer due to the spool geometry into account. In order to calculate the twist we consider the left-handed helix $\vec{r}(\alpha) = R^{(n)}(\cos\alpha, -\sin\alpha, \gamma\alpha)$ with the pitch ratio $\gamma = p/(2\pi R^{(n)})$ and parametrized by an angle α in the $x-y$ plane of a coordinate system with the z-direction aligned with the histone core axis $\vec{c}$. The corresponding unit tangent vector $\vec{t}(\alpha)$ and the unit normal vector $\vec{n}(\alpha)$ of the helix are given by $\vec{t}(\alpha) = (1+\gamma^2)^{-1/2}(-\sin\alpha, \cos\alpha, \gamma)$ and $\vec{n}(\alpha) = -\vec{b} = (-\cos\alpha, \sin\alpha, 0)$. If we consider two adjacent segments at the positions $\vec{r}(\alpha_0)$ and $\vec{r}(-\alpha_0)$ without loss of generality, the twist angle $\Delta\tau = \tau_1 + \tau_2$ between the two segments is the sum of the angle τ_1 between the vector $\vec{p} = \vec{t}(\alpha_0) \times \vec{t}(-\alpha_0)$ and the normal vector $\vec{n}(\alpha_0)$ and the angle τ_2 between $\vec{n}(-\alpha_0)$ and $\vec{p}$:

$$\Delta\tau = -2\arccos\left(-\frac{h}{\sqrt{(l_0\gamma)^2 + 4R^{(n)}R^{(n)}\sin^2\alpha_0}}\sin\alpha_0\right) + \pi \tag{8}$$

The vector $\vec{a}$ is then finally obtained by rotation of the vector $\vec{b}$ about the angle $\tau = \Delta\tau/(2\alpha_0)\alpha$ around $\vec{c} \times \vec{b}$.

Forces and Torques. The forces and torques are calculated as the partial derivatives of the energy over the system coordiantes. The energy is given by the sum of the individual energies defined in preceding sections. The complete system is specified by the segment verticies $\vec{r}_i$, the angle ϕ_i of rotation of the local vector basis $(\vec{f}_i, \vec{g}_i, \vec{e}_i)$ around the $\vec{e}_i$ axis, the histone core position $\vec{r}^{(n)}$ and the histone core axis $\vec{c}$. The expressions for forces and torques acting on the polymer chain due to DNA−DNA interaction have been calculated by Klenin et al.[1] Forces and torques acting on DNA and histone due to the DNA−histone core interaction are derived in the Appendix.

Hydrodynamic Interactions. Hydrodynamic interactions were introduced to the model by attaching beads to each chain vertex and a bead representing the histone core, an approach which has been widly used to calculate hydrodynamics of DNA segments.[17,18] The hydrodynamic diffusion tensor $\mathbf{D}$ represents the hydrodynamic interaction and is composed of 3×3 submatricies $\mathbf{D}_{ij}$, which describe the interactions between the individual beads i and j with radius of σ_i and σ_j, respectively. Acceptable values for the radius σ_i are the hydrodynamic DNA

bead radius a for a DNA bead and the hydrodynamic histone core bead radius $r_{HD}^{(\eta)}$ for the histone core bead. The DNA bead radius a is adjusted such that the diffusion coefficient of n beads placed equidistantly in a row with distance l_0 equals the diffusion coefficient of a cylinder of radius r_{HD} and length nl_0. The diffusion coefficient of a cylinder can be calculated as described in refs 2 and 3 while the diffusion coefficient for the string of beads is given in ref 4. The applied translational−translational self-diffusion matrix is

$$\mathbf{D}_{ii}^{tt} = \frac{k_B T}{6\pi\eta\sigma_i}\mathbf{I} \tag{9}$$

For the hydrodynamic interaction between different beads $i \neq j$ two cases—overlapping and nonoverlapping beads—have to be considered. The beads are called overlapping, when the spatial separation r_{ij} between the beads is less than $\sigma_i + \sigma_j$. The resulting modifided Rotne−Prager tensor is

$$\mathbf{D}_{ij}^{tt} = \begin{cases} \frac{k_B T}{8\pi\eta r_{ij}}\left[\left(1 + \frac{\sigma_i^2 + \sigma_j^2}{3r_{ij}^2}\right)\mathbf{I} + \left(1 + \frac{\sigma_i^2 + \sigma_j^2}{3r_{ij}^2}\right)\frac{\vec{r}_{ij} \otimes \vec{r}_{ij}}{r_{ij}^2}\right] & r_{ij} \geq \sigma_i + \sigma_j \\ \frac{k_B T}{8\pi\eta\sigma_{eff}}\left[\left(1 + \frac{9r_{ij}}{32\sigma_{eff}}\right)\mathbf{I} + \frac{3}{32\sigma_{eff}}\frac{\vec{r}_{ij} \otimes \vec{r}_{ij}}{r_{ij}^2}\right] & r_{ij} \geq \sigma_i + \sigma_j \end{cases} \tag{10}$$

where for beads with unequal radii $\sigma_{eff} = [(\sigma_i^2 + \sigma_j^2)/2]^{1/2}$. If the beads have equal radii σ_{eff} is simply replaced by the respective bead radius. As there does not exist a rigorously analytical solution for overlapping beads with unequal radii, an intermediate value σ_{eff} between the different bead radii has been used throughout the simulations for this case. Similar expressions have been proposed in refs 16 and 17. Rotation is treated differently for the nucleosome core bead and DNA beads. The rotation diffusion matrix for the nucleosome core bead is defined as

$$\mathbf{D}_{ii}^{rr} = \frac{k_B T}{8\pi\eta\sigma_i^3}\mathbf{I} \tag{11}$$

The coupling between rotation and translation for different beads is given by

$$\mathbf{D}_{ij}^{rt} = \begin{cases} \frac{k_B T}{8\pi\eta r_{ij}^3}\epsilon \cdot \vec{r}_{ij} & r_{ij} \geq \sigma_i + \sigma_j \\ \frac{k_B T}{8\pi\eta(\sigma_i + \sigma_j)^2}\epsilon \cdot \frac{\vec{r}_{ij}}{r_{ij}} & r_{ij} < \sigma_i + \sigma_j \end{cases} \tag{12}$$

and the product $\epsilon \cdot \vec{r}_{ij}$ is defined, with the vector $\vec{r}_{ij}$ in Cartesian coordinates (x_{ij}, y_{ij}, z_{ij}), in the following way:

$$\epsilon \cdot \vec{r}_{ij} = \begin{pmatrix} 0 & z_{ij} & -y_{ij} \\ -z_{ij} & 0 & x_{ij} \\ y_{ij} & -x_{ij} & 0 \end{pmatrix} \tag{13}$$

For beads representing DNA rotational movement is restricted to rotation about the $\vec{e}_i$-axis. We treat therefore the rotation of a individual DNA beads as hydrodynamically decoupled from the remaining beads. The corresponding rotational diffusional matrix is given by

$$D_{rot} = \frac{k_B T}{4\pi\eta r_{HD}^2 l_0} \tag{14}$$

Brownian Dynamics Algorithm. A second-order Brownian dynamics algorithm has been applied in the simulation to calculate the consecutive chain and histone core conformations. The conformation of the system at time t is denoted by the super vector $\vec{R} = \{\vec{r}_i(t), \vec{r}^{(n)}(t), \vec{c}(t)\}$ keeping track of the bead positions $\vec{r}_i$, the histone core position $\vec{r}^{(n)}$ and the histone core axis $\vec{c}$ at time t. The super vector $\vec{A} = \{\vec{F}_i, \vec{F}^{(n)}, \vec{T}^{(n)}\}$ is composed of the corresponding forces $\vec{F}_i$, $\vec{F}^{(n)}$, and torque $\vec{T}^{(n)}$ acting on the tth DNA segment and histone core and T_i is the torque acting on the ith DNA segment. In the first half-step the predicted vector $\vec{R}'$ and the rotation angles ϕ_i at time $t + \Delta t$ are calculated according to

$$\vec{R}_i'(t + \Delta t) - \vec{R}_i(t) = \sum_{j=0}^{N} \mathbf{D}_{ij}(t)\frac{\vec{A}_j(t)}{k_B T}\Delta t + \vec{X}_i \tag{15}$$

$$\phi_i'(t + \Delta t) - \phi_i(t) = D_{rot}\frac{T_i(t)}{k_B T}\Delta t + \Phi_i \tag{16}$$

The random fluctuations $\vec{X}_i$ and Φ_i, with the following covariances

$$\langle \vec{X}_i \vec{X}_i^T \rangle = 2\mathbf{D}_{ij}\Delta t \tag{17}$$

$$\langle \Phi_i \Phi_j \rangle = 2D_{rot}\Delta t \tag{18}$$

are calculated by a Cholesky factorization of the hydrodynamic diffusion matrix $\mathbf{D} = \mathbf{L}\mathbf{L}^T$, where $\mathbf{L}$ is a lower triangular matrix. In the second half-step the final system coordinates $\vec{R}_i(t + \Delta t)$, ϕ_i are obtained from the forces and torques $\vec{A}_j'$ calculated at the predicted system coordinates at time $t + \Delta t$:

$$\vec{R}_i(t + \Delta t) - \vec{R}_i'(t + \Delta t) = \sum_{j=0}^{N} \mathbf{D}_{ij}(t)\frac{-\vec{A}_j(t) + \vec{A}_j'(t + \Delta t)}{2k_B T}\Delta t \tag{19}$$

$$\phi_i(t + \Delta t) - \phi_i'(t + \Delta t) = D_{rot}\frac{-T_i(t) + T_i'(t + \Delta t)}{2k_B T}\Delta t \tag{20}$$

The hydrodynamic diffusion tensor $\mathbf{D}$ is not updated in every simulation step but only every 500 simulation steps to speed up the simulation.[1]

An initial conformation is created, where all segments are ordered in a straight line and the histone core $\vec{r}^{(n)}$ is positioned at a distance $R^{(n)}$ from the middle chain segment $\vec{r}_{N/2}^{(m)}$ (Figure 1a). The starting conformation is obtained by applying at first a constant external force of 20 pN to the DNA end segments until a maximum of 3 segments are interacting with the histone core for 10^5 simulation steps (Figure 1b). The ith segment is termed interacting if the interaction distance $|\vec{R}_i|$, is within the cutoff distance r_0. Then this extended conformation is relaxed

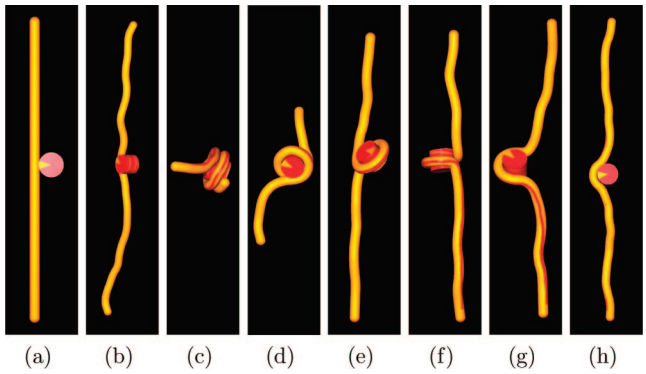

Figure 1. Nucleosome conformations are shown during the initialization: (a) initial conformation, (b) extended conformation with an external applied force of 20 pN and the conformation at different simulation times ($v = 0.1$ cm s^{-1}); (c) relaxed starting conformation at $t = 0$, (d) 46.0, (e) 83.5, (f) 84.0, (g) 84.3, and (h) 100 μs.

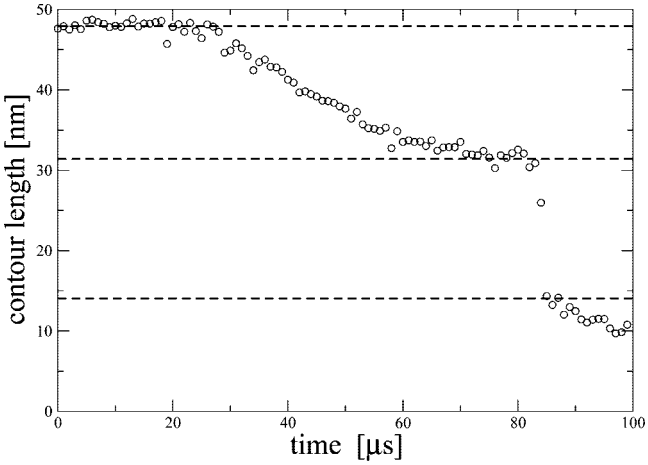

Figure 2. Representative contour length curve of adsorbed DNA onto the histone core (*circles*) is shown in dependence on time. At the starting conformation ~48 nm DNA are adsorbed. The pulling of the DNA at a constant velocity ($v = 0.1$ cm s^{-1}) displays a gradual release of DNA from the outer DNA turn of the nucleosome core particle. The second turn of DNA is released in an disruptive event on a time scale below 1 μs.

in 10^8 simulation steps with no external forces to an equilibrated conformation, where DNA makes a superhelix around the protein (Figure 1c). Data has been collected at time intervals of 6 ns for fast stretching velocities ($v > 0.005$ cm s^{-1}) and 600 ns for slow stretching velocities ($v \leq 0.005$ cm s^{-1}). For each parameter set, 15 simulations runs have been calculated. The stretching simulations have been calculated on a AMD Opteron 2.4 Ghz system, such that a 3.6 ms Brownian dynamics simulation with 6×10^8 steps took ~1 week of computer time.

Results

Force-Extension Curves. The starting point for the BD simulation is an equilibrated conformation, where DNA with a contour length of 48−49 nm is wrapped tightly around the protein. The contour length of the adsorbed DNA is defined as the total length of the interacting segments. From time $t = 0$, the DNA end segments are displaced relative to each other with a constant stretching velocity $\vec{v}$. DNA is released in three steps as shown in Figure 2: initially the pulling of the DNA ends releases gradually the outer turn of ~16 nm nucleosomal DNA from the histone core. In contrast the inner turn unwinds in a sudden event, where the histone core has to rotate out-of-plane

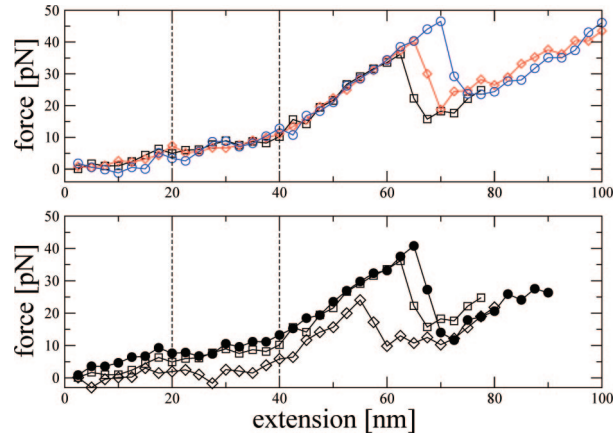

Figure 3. Representative force-extension curves have been recorded during the stretching simulation. (top) Stretching velocities ranging from $v = 0.0025$ (*square*), 0.01 (*diamond*), to 0.1 cm s^{-1} (*circle*) have been used at a constant adsorption energy density $\epsilon = 8\ k_BT$ nm^{-1}. (bottom) Figure showing force-extension curves for the case of the bare DNA charge ($\epsilon = 6$ (*diamond*) and 8 k_BT nm^{-1} (*square*) and the renormalized DNA charge $\epsilon = 6\ k_BT$ nm^{-1} (*filled circle*)). The stretching velocity has been held constant at $v = 0.0025$ cm s^{-1}.

to reach the extended state (Figure 1d−g). In this disruptive event ~17−22 nm of DNA desorb, still leaving ~11−14 nm of DNA attached, as the bending energy of the attached DNA segments is exceeded by the energetic gain due to the DNA−histone core interaction.

During the simulation the force at the DNA end segments F and the extension x (the DNA end-to-end distance in direction of the stretching velocity) are calculated. In order to obtain force-extension curves, the forces are averaged over the extension with a bin width of the segment equilibrium length l_0. Simulations have been carried out at different stretching velocities v and at different adsorption energy density ϵ as shown in Figure 3. Histone modification, e.g. acetylation of the tails or total removal of tails, can reduce the positive charge interacting with the DNA, therefore reducing the interaction between protein and DNA.[19,20] Studies showed also sequence-dependent binding affinities of DNA to the histone core proteins.[23] The parameter ϵ is used in this study to reflect the varying strength of interaction. The first part of the force-extension ($x < 20$ nm) is associated with the pulling of the free, nonadsorbed linker DNA. After this, the force-extension curves exhibit two distinct regimes, a low-force regime and a high-force regime at a greater extension. The low-force regime can be identified with the unwrapping of the outer DNA turn at nearly constant force. A mean average unwrapping force for the outer turn of DNA has been calculated from the obtained forces by chi-square fitting (20 nm $\leq x <$ 40 nm) at the force plateau, yielding 7.3 pN ($\epsilon = 8\ k_BT$ nm^{-1}) and 2.1 pN ($\epsilon = 6\ k_BT$ nm^{-1}). In the case of bare DNA charge, Coulombic repulsion between the DNA turns facilitates unwrapping, such that the outer DNA turn is accessible to proteins. In comparison the calculated forces for a renormalized DNA charge are higher: 6.6 pN ($\epsilon = 5\ k_BT$ nm^{-1}) and 9.6 pN ($\epsilon = 6\ k_BT$ nm^{-1}). The force at the DNA ends increases linearly with the extension in the high-force regime until the inner DNA turn unwraps abruptly, which is accompanied by a sudden drop in the calculated force. The local maximum of the force at rupture is referred to as rupture force. The linear continuation after the force peak is due to the harmonic contribution of the stretching energy.

The linearity of the force-extension curve before the force peak allows us to calculate the corresponding force loading rate

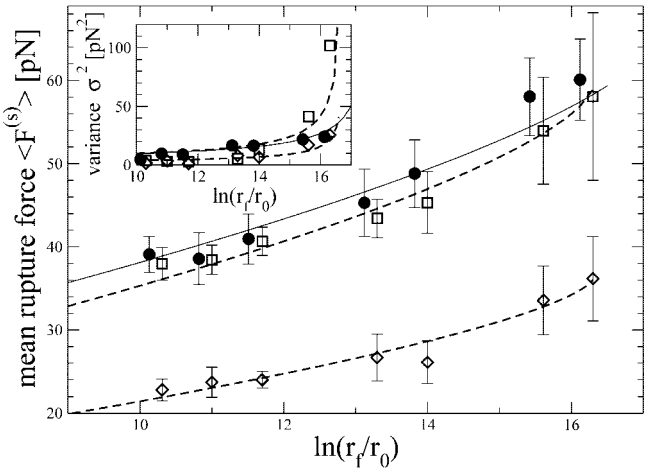

Figure 4. Simulated mean rupture forces as a function of the force loading rate are shown for an adsorption energy density $\epsilon = 8$ (*square*) and 6 k_BT nm^{-1} (*filled circle*) for the renormalized case. Solutions of the mean rupture forces derived from the microscopic theory (*line*) with parameters according to Table 2 are drawn in the figure. $r_0 = 1$ pN s^{-1} is an arbitrary scale on the force loading rate axis. (inset) Simulated variance of mean rupture force (*square, filled circle*) and the analytical solution of the mean rupture force variance for the microscopic theory (*line*) with the same parameters.

TABLE 1: Simulation Parameter Values

parameter	description	value
Δt	simulation time step	6.0 ps
T	temperature	293.15 K
I	ionic strenght	150 mM
η	viscosity	1.0×10^{-3} Pa s
D	dielectric constant	80.18
N	number of segments	30
l_0	equilibrium segment length	2.5 nm
δ	stiffness parameter	0.16
B	Kuhn length	100 nm
C	torsional rigidity constant	61.8 k_BT
r_{HD}	hydrodynamic DNA radius	1.2 nm
$r_{HD}^{(n)}$	hydrodynamic histone core radius	3.0 nm
$R^{(n)}$	histone core radius	4.18 nm
Θ_0	critical potential angle	$\pi/2$
k_0	potential coefficient	0.1
r_0	potential cutoff distance	0.5 nm

$r_f = dF/dt$ from the stretching velocity v. The force loading rate is simply proportional to the stretching velocity $r_f = k_{eff}v$, where k_{eff} is the effective spring constant. The effective spring constant $k_{eff} = dF/dx$ has been calculated by chi-square fitting from the average slope of the force-extension curves before rupture. In the simulations, the effective spring constant is estimated to have a value in the range of $k_{eff} \sim 1.0-1.2$ pN nm^{-1}. Simulation runs have been performed for each adjusted stretching velocity and adsorption energy density. The ruputure forces are averaged to calculate the mean rupture force $\langle F^{(s)}\rangle$ and the variance of force $(\sigma_F^{(s)})^2$. The collected data shows that with decreasing stretching velocity v and/or adsorption energy density ϵ, the mean rupture force decreases as well. The dependence of the simulated mean rupture force on the force loading rate r_f and the adsorption energy density ϵ is shown in Figure 4.

A stepwise release of DNA in three stages has likewise been observed in experimental studies.[13,15] In the experimental setup, forces below 15 pN are needed to unwrap the outer turn, and at forces above 15 pN, the onset of the linear slope has been measured. The effect that DNA is kept bound at the dyad axis of the histone octamers after relaxation of the external force has been reported in ref 15.

TABLE 2: Microscopic Theory Parameters

	renormalized DNA charge		bare DNA charge	
ϵ [k_BT nm^{-1}]	5.0	6.0	6.0	8.0
d [nm]	3.38	2.54	4.06	2.54
k_{off} [s^{-1}]	5.85×10^{-5}	1.7×10^{-5}	2.1×10^{-4}	7.9×10^{-5}
E_b [k_BT]	25.2	27.1	24.2	24.7

In order to explain the high rupture forces, strong chemical interactions sites at specific positions in the proximity of the nucleosome dyad axis have been postulated by Brower−Toland et al.[15] In contrast, in this simulation model the DNA−protein interaction is uniformally distributed along the superhelical path, which shows that this assumption is sufficient to reproduce the characteristic force-extension curves. The result is in agreement with the findings of Kulic et al.[14] who found in an analytical model that the kinetic protection of the inner DNA turn from unwrapping is a consequence of the toroidal geometry of the nucleosome. We find also that for the case of the bare DNA charge the Coulombic repulsion between the two DNA strands reduces the rupture forces significantly in comparison to the case of renormalized DNA charge.

Microscopic Theory. We analyze the data with a method which has been proposed by Dudko et al.[9] and described in a general form in ref 10, in order to extract information about kinetics in single-molecule pulling experiments. In their model of dynamically forced escape, a specific energy surface, e.g. a linear-cubic energy surface $U_0(\alpha)$ with an energy minimum at the reaction coordinate $\alpha = 0$ and an energy barrier at a reaction distance $\alpha = d$, is perturbated in the presence of an applied force field $-F\alpha$, in which the external force F increases monotonically with time. It is assumed that for high forces all smooth combined energy surfaces can be well represented by a cubic polynomial. The rate constant $k(F)$ for transition of the energy barrier can be calculated with the use of the Kramers theory[11] from the force-modulated potential, which then allows to derive the distribution of rupture forces $p(F|r_f)$ in dependence on the force loading rate r_f. In the limit of high forces near the critical force, at which the energy barrier vanishes, the expressions for the mean rupture force

$$\langle F^{(a)}\rangle = \frac{E_b}{\nu d}\left(1 - \left(\frac{1}{E_b}\ln\frac{k_{off}\exp(E_b + \gamma)}{dr_f}\right)^{\nu}\right) \quad (21)$$

and the variance of the rupture force

$$[\sigma_F^{(a)}]^2 = \frac{\pi^2}{6d^2}\left[\frac{1}{E_b}\ln\frac{k_{off}\exp(E_b + \tilde{\gamma})}{dr_f}\right]^{2\nu-2} \quad (22)$$

can be derived. The term $\tilde{\gamma}$ has approximately a numerical value of 1.064 and ν is set to a value of $^2/_3$ for a linear-cubic energy surface. The reaction distance d between the bound state and the energy barrier peak, the energy barrier E_b, and the rate constant for transition of the energy barrier at zero external force k_{off} are the three free parameters of the formulas, which can be adjusted to the rupture force data. The variance data has been included in order to further narrow the parameter value space. The deviation of the analytical solution for the mean rupture force eq 21 with a specified set of paramters from the simulation

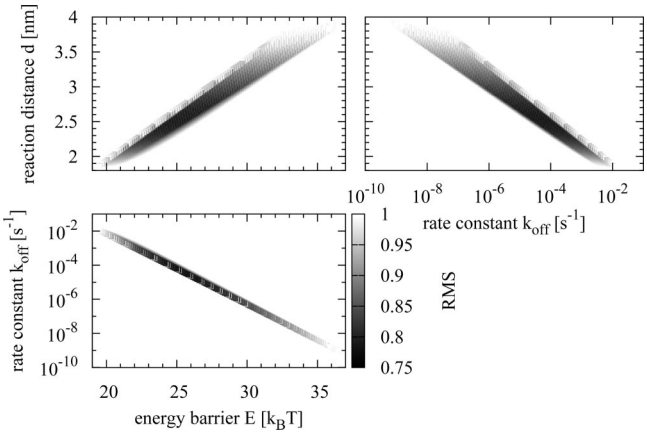

Figure 5. Maximum of the root-mean-square deviations for the mean rupture force RMS_F and for the standard deviations of the mean rupture force RMS_σ is shown ($\epsilon = 8\ k_BT\ nm^{-1}$) for the bare DNA charge. The projection onto planes of the 3-dimensional parameter values space allows the identification of bounds on the parameters E_b, d, and k_{off}.

results can be quantified by the χ_F^2 function. χ_F^2 is defined as the sum

$$\chi_F^2 = \sum_{r_f} \frac{[\langle F^{(s)}(r_f)\rangle - \langle F^{(a)}(r_f)\rangle]^2}{[\sigma_F^{(s)}(r_f)]^2} \tag{23}$$

where $\langle F_i^{(s)}\rangle$ and $\langle F_i^{(a)}\rangle$ are the simulated and calculated average rupture forces at force loading rates r_f, respectively, and the quadratic deviations $[\langle F_i^{(s)}\rangle - \langle F_i^{(a)}\rangle]^2$ are weighted by the variance of the simulated rupture force $[\sigma_{F_i}^{(s)}]^2$, as the variance is nonuniform for different force-loading rates. In analogy a quantity χ_σ^2 can be defined for the standard deviations of the simulated mean rupture forces:

$$\chi_\sigma^2 = \sum_{r_f} \frac{[\sigma^{(s)}(r_f) - \sigma^{(a)}(r_f)]^2}{\sigma_\sigma^2} \tag{24}$$

Here $\sigma_i^{(s)}$ and $\sigma_i^{(a)}$ denote the simulated and calculated standard deviations, while σ_σ is the uniform statistical error of the standard deviation. If we assume statistical errors of the standard deviations of σ_σ, defined as a 20% relative error of the maximal standard deviation (corresponding to ~2 pN at $\epsilon = 8\ k_BT\ nm^{-1}$), root-mean-square deviations for the mean force $RMS_F = (\chi_F^2/n)^{1/2}$ and for the standard deviations of the mean force $RMS_\sigma = (\chi_\sigma^2/n)^{1/2}$ can be calculated. The maximum of the root-mean-square deviation $RMS = \max(RMS_F, RMS_\sigma)$ is used to find the parameter values, which are simultaneously consistent with the simulated mean rupture forces and standard deviations of the mean rupture force. Therefore the root-mean-square deviation RMS has been evaluated at discrete points in the parameter value space (E_b, d, $\log_{10}(k_{off})$), separated equidistantly ($\Delta E_b = 0.05\ k_BT$, $\Delta d = 0.02$ nm, $\Delta\log_{10}(k_{off}) = 0.03$). If we set as a tolerance threshold a RMS deviation of unity, we estimate $19.5\ k_BT \le E_b \le 36.3\ k_BT$, $10^{-9}\ s^{-1} \le k_{off} \le 10^{-2}\ s^{-1}$, and 1.9 nm $\le d \le$ 3.9 nm (at $\epsilon = 8\ k_BT\ nm^{-1}$, bare DNA charge) with minimal deviations for an energy barrier $E_b = 24.7\ k_BT$, rate constant $k_{off} = 7.9 \times 10^{-5}\ s^{-1}$, and a reaction distance $d = 2.54$ nm as listed in Table 2 (See Figure 5). Corresponding mean rupture force curves and force variances are shown in Figure 4. Figure 5 shows that the parameters are correlated to each other and parameter value space can be further reduced

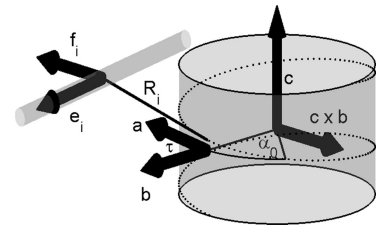

Figure 6. Schematic representation of the histone core model. The histone core is represented as a cylinder with the symmetry axis $\vec{c}$. A superhelix (*dotted line*) of 1.75 turns is parametrized by the angle α in the plane perpendicular to the $\vec{c}$-axis. The distance dependence of the DNA−histone core potential is given by the interaction distance $|\vec{R}_i|$ between the middle point of the ith segment and the closest point on the superhelix, while the vector $\vec{b}$ is the projection of $\vec{r}_i$ onto the plane perpendicular to $\vec{c}$. At each point of the superhelix, a vector $\vec{a}$ is defined, which takes the DNA twist due to the spool geometry into account. The vector $\vec{a}$ is obtained by rotation of the vector $\vec{b}$ by an angle τ about the rotation axis $\vec{c} \times \vec{b}$.

by assuming a smaller relative error of the maximal standard deviation. A widely used approach to analyze experimental data is the phenomenological description of force-induced rupture based upon Bell's equation[12] for the rate constant for rupture under an external time-dependent force $F(t)$. But at high-force loading rates used in the simulations, the microscopic theory accounts far better for the nonlinearity of the mean rupture force and the nonconstant variance, which contradict the predictions of the phenomenological theory. It is consistent with the statement that eq 21 emerges as limiting case for high-force loading rates of a general solution for forced barrier crossing in single molecules.[22]

The analytical solution of the microscopic theory for the mean rupture force with the obtained parameters allows to extrapolate to slower force loading rates into the range of typical experimental stretching experiments. The extrapolation of the analytical solution of eq 21 is justified, as it has been checked that for the parameters no deviations from the general solution for the complete spectrum of force loading rates[22] in the range of intermediate force loading rates occur.

In the experimental work of Pope el al.,[13] reconstituted chromatin fibers have been studied at different loading rates at salt conditions of 150 mM NaCl comparable to the settings in this simulation. They observed unwrapping events with discrete force peaks and step lenghts of extension centered at 60 nm, which have been associated with the disruption of entire nucleosomes, and at 30 nm, corresponding to partial nucleosome disruption events. Three different rupture force distributions with individual energy barriers and rate constants have been identified. A high-force population has been related to the presence of a linker histone B4, while the remaining two rupture force distributions with no linker histone occur at a low and a high force loading rate, respectively. The analytical solution at $\epsilon = 8\ k_BT\ nm^{-1}$ for the case of bare DNA charge displays the best approximation to the experimental data only for the low-force loading rate distribution (see Figure 7), which is expected to represent the unperturbed natural system best. This could indicate that the high-force loading rate distribution has a different reaction pathway. According to ref 9, internal degrees of freedom can explain for multiple rupture force distributions, which can not be described within our simulation model e.g. release of a H2A−H2B dimer and formation of subnucleosomal particles in the unwrapping process as proposed in the study.[13]

Conclusions

A new model for the nucleosome is described here allowing to simulate stretching experiments. The DNA is modeled using

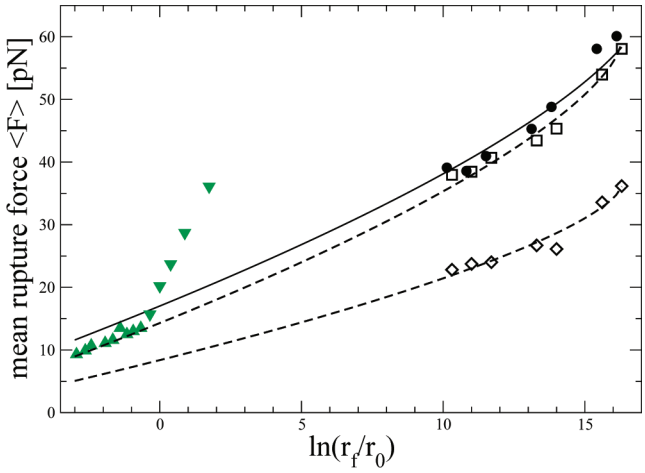

Figure 7. Extrapolation of the analytical solution with to intermediate force loading rates are shown for the bare DNA charge ((*diamond*) $\epsilon = 6\ k_BT\ \mathrm{nm}^{-1}$, (*square*) $\epsilon = 8\ k_BT\ \mathrm{nm}^{-1}$) and the renormalized DNA charge ((*filled circle*) $\epsilon = 6\ k_BT\ \mathrm{nm}^{-1}$). Experimental data taken from ref 13 is included in the figure (low-force loading rate (*triangle up*) and high-force loading rate (*triangle down*) mean rupture force distribution).

an approach developed for linear and circular polymers,[1] which represents DNA as a chain of linear segments. Mechanical properties are included via harmonic potentials for bending, stretching, and twisting of the segments and electrostatics is treated within a Debye−Hückel approach. The histone core is essentially based on the nucleosome geometry known from X-ray crystallography and the interaction with the DNA segments is modeled with an attractive short-ranged potential. The dynamics of the nucleosome are calculated with a second-order Brownian dynamics algorithm with included hydrodynamics. The unwrapping process has been systematically examined by pulling at the DNA end segments with a constant velocity. The simulated force-extension curves displayed the same distinctive regimes that have been previously reported in experimental studies. The outer DNA turn unwraps at low forces, which are in the range of experimental results. The Coulombic repulsion between the two adjacent DNA turns facilitates the exposure of the DNA. Rupture forces at which the second DNA turn unwinds in a disruptive event has been analyzed with a microscopic theory, to extract relevant energy parameters and kinetic rate constants of the transition. The analytical solutions extrapolated to intermediate force loading rates have been compared to experimental data at comparable ionic conditions[13] and match well for an adsorption energy density of $\epsilon = 8\ k_BT\ \mathrm{nm}^{-1}$ or about 2.7 k_BT per basepair. We conclude that the toroidal geometry of the nucleosome with a nonspecific, short-ranged DNA−protein interaction is sufficient to explain for the general results of stretching experiments. A further improvement could incorporate localized interaction sites for the DNA−protein interaction, modulating the uniform adsorption energy density profile, which would likely lead to more specific predictions of the nucleosome dynamics.

Appendix

In this Appendix, forces and torques due to the DNA−histone core interaction are calculated as the partial derivatives of the DNA−histone core interaction energy $E_i^{(n)}$ over the system coordinates. The force $\vec{F}_i^{(n)}$ acting on the ith segment can be expressed as the sum

$$\vec{F}_i^{(n)} = \vec{F}_{i,\mathrm{next}}^{(\mathrm{act})} + \vec{F}_{i,\mathrm{prev}}^{(\mathrm{act})} - \vec{F}_{i,\mathrm{next}}^{(\mathrm{rot})} + \vec{F}_{i,\mathrm{prev}}^{(\mathrm{rot})} \tag{25}$$

The contributions to the DNA−histone core interaction force acting on the ith vertex from the ith segment are $\vec{F}_{i,\mathrm{next}}^{(\mathrm{act})}$ and $\vec{F}_{i,\mathrm{next}}^{(\mathrm{rot})}$:

$$\vec{F}_{i,\mathrm{next}}^{(\mathrm{act})} = \begin{cases} -\dfrac{U_0}{2r_0}\dfrac{\partial|\vec{R}_i|}{\partial\vec{r}_i^{(m)}}\left[\dfrac{\Theta_0-\Theta_i}{\Theta_0}(1-k_0)+k_0\right] & \\ +\dfrac{U_0}{2}\dfrac{r_0-|\vec{R}_i|}{r_0}\dfrac{1-k_0}{\Theta_0}\dfrac{1}{\sqrt{1-(\vec{a}_i\vec{f}_i)^2}}\dfrac{\partial(\vec{a}_i\cdot\vec{f}_i)}{\partial\vec{r}_i^{(m)}} & \Theta_i < \Theta_0 \\ -\dfrac{U_0}{2r_0}k_0\dfrac{\partial|\vec{R}_i|}{\partial\vec{r}_i^{(m)}} & \Theta_i \geq \Theta_0 \end{cases} \tag{26}$$

and

$$\vec{F}_{i,\mathrm{next}}^{(\mathrm{rot})} = \begin{cases} U_0\dfrac{r_0-|\vec{R}_i|}{r_0}\dfrac{1-k_0}{\Theta_0}\dfrac{1}{\sqrt{1-(\vec{a}_i\cdot\vec{f}_i)^2}}\dfrac{\vec{e}_i\times(\vec{a}_i\times\vec{f}_i)}{|\vec{s}_i|} & \Theta_i < \Theta_0 \\ 0 & \Theta_i \geq \Theta_0 \end{cases} \tag{27}$$

where

$$\frac{\partial(\vec{a}_i\cdot\vec{f}_i)}{\partial\vec{r}_i^{(m)}} = \vec{f}_i(\tau[\vec{c}\times\vec{b}_i]\times\vec{a}_i + [\vec{c}\times\vec{a}_i])\frac{\vec{c}\times\vec{a}_i}{|\vec{r}_i^{(m)}-\vec{r}^{(n)}|}$$

$$\frac{\partial|\vec{R}_i|}{\partial\vec{r}_i^{(m)}} = \frac{1}{|\vec{R}_i|}\left(-\vec{R}_i + (R^{(n)}\vec{R}_i\cdot[\vec{c}\times\vec{b}_i] - p\vec{R}_i\cdot\vec{c})\frac{\vec{c}\times\vec{b}_i}{|\vec{r}_i^{(m)}-\vec{r}^{(n)}|}\right)$$

The analogous contributions to the DNA−histone core interaction force acting on the ith vertex from the $(i-1)$th segment are $\vec{F}_{i,\mathrm{prev}}^{(\mathrm{act})}$ and $\vec{F}_{i,\mathrm{prev}}^{(\mathrm{rot})}$, which can be obtained by substituting the ith terms with the corresponding $(i-1)$th terms in the respective eqs 26 and 27.

The torque $T_i^{(n)}$ on the ith segment is defined as

$$T_i^{(n)} = \begin{cases} U_0\dfrac{r_0-|\vec{R}_i|}{r_0}\dfrac{1-k_0}{\Theta_0}(1-(\vec{a}_i\cdot\vec{f}_i)^2)^{-1/2}\vec{a}_i[\vec{e}_i\times\vec{f}_i] & \Theta_i < \Theta_0 \\ 0 & \Theta_i \geq \Theta_0 \end{cases} \tag{28}$$

The counterforce $\vec{F}^{(n)}$ and the countertorque $\vec{T}^{(n)}$ acting on the histone core are then given by

$$\vec{F}^{(n)} = -\sum_{i=0}^{N}(\vec{F}_{i,\mathrm{prev}}^{(\mathrm{act})} + \vec{F}_{i,\mathrm{next}}^{(\mathrm{act})}) \tag{29}$$

$$\vec{T}^{(n)} = -\sum_{i=0}^{N}(\vec{r}_i^{(m)} - \vec{r}^{(n)}) \times (\vec{F}_{i,\mathrm{prev}}^{(\mathrm{act})} + \vec{F}_{i,\mathrm{next}}^{(\mathrm{act})}) \tag{30}$$

References and Notes

(1) Klenin, K. V.; Langowski, J. *Biophys. J.* **1998**, *74*, 780–788.

(2) Tirado, M. M.; Garcia de la Torre, J. *J. Chem. Phys.* **1979**, *71*, 2581–2587.
(3) Tirado, M. M.; Garcia de la Torre, J. *J. Chem. Phys.* **1980**, *73*, 1986–2587.
(4) Hagerman, P. J.; Zimm, B. H. *Biopolymers* **1981**, *20*, 1481–1502.
(5) Rotne, J.; Prager, S. *J. Chem. Phys.* **1969**, *50*, 4831–4837.
(6) Luger, K.; Maeder, A. W.; Richmond, R. K.; Sargent, D. F.; Richmond, T. J. *Nature* **1997**, *389*, 251–260.
(7) Davey, C. A.; Sargent, D. F.; Luger, K.; Maeder, A. W.; Richmond, T. J. *J. Mol. Biol.* **2002**, *319*, 1097–1113.
(8) Richmond, T. J.; Davey, C. A. *Nature* **2003**, *423*, 145–150.
(9) Dudko, O. K.; Filippov, A. E.; Klafter, J.; Urbakh, M. *Proc. Natl. Acad. Sci.* **2003**, *100*, 11378–11381.
(10) Dudko, O. K.; Hummer, G.; Szabo, A. *Phys. Rev. Lett.* **2006**, *96*, 108101.
(11) Kramers, H. A. *Physica (Utrecht)* **1940**, *7*, 284.
(12) Bell, G. I. *Science* **1978**, *200*, 618–627.
(13) Pope, L. H.; Bennink, M. L.; van Leijenhorst-Groener, K. A.; Nikova, D.; Greve, J.; Marko, J. F. *Biophys. J.* **2005**, *88*, 3572–3583.
(14) Kulić, I. M.; Schiessel, H. *Phys. Rev. Lett.* **2004**, *92*, 228101.
(15) Brower-Toland, B. D.; Smith, C. L.; Yeh, R. C.; Lis, J. T.; Peterson, C. L.; Wang, M. D. *Proc. Natl. Acad. Sci.* **2002**, *99*, 1960–1965.
(16) Carrasco, B.; de la Torre, J. G.; Zipper, P. *Eur. Biophys. J.* **1999**, *28*, 510–515.
(17) Arya, G.; Zhang, Q.; Schlick, T. *Biophys. J.* **2006**, *91*, 133–150.
(18) Stigter, D. *Macromolecules* **2000**, *33*, 8878–8889.
(19) Brower-Toland, B.; Wacker, D. A.; Fulbright, R. M.; Lis, J. T.; Kraus, W. L.; Wang, M. D. *J. Mol. Biol.* **2005**, *346*, 135–146.
(20) Wolffe, A. P.; Hayes, J. J. *Nucleic Acids Res.* **1999**, *27*, 711–720.
(21) Manning, G. S. *J. Chem. Phys.* **1969**, *51*, 924.
(22) Friddle, R. W. *Phys. Rev. Lett.* **2008**, *100*, 138302.
(23) Lowary, P. T.; Widom, J. *J. Mol. Biol.* **1998**, *276*, 19–42.

JP806137E